Nanoscale

RSC Publishing

PAPER

Carbon doping of InSb nanowires for high-performance p-channel field-effect-transistors†

Cite this: *Nanoscale*, 2013, **5**, 9671

Zai-xing Yang,‡[a] Ning Han,‡[ac] Fengyun Wang,[ac] Ho-Yuen Cheung,[b] Xiaoling Shi,[a] SenPo Yip,[ac] TakFu Hung,[a] Min Hyung Lee,[d] Chun-Yuen Wong[b] and Johnny C. Ho*[ac]

Received 14th June 2013
Accepted 5th August 2013

DOI: 10.1039/c3nr03080f

www.rsc.org/nanoscale

Due to the unique physical properties, small bandgap III–V semiconductor nanowires such as InAs and InSb have been extensively studied for the next-generation high-speed and high-frequency electronics. However, further CMOS applications are still limited by the lack of efficient p-doping in these nanowire materials for high-performance p-channel devices. Here, we demonstrate a simple and effective *in situ* doping technique in the solid-source chemical vapor deposition of InSb nanowires on amorphous substrates employing carbon dopants. The grown nanowires exhibit excellent crystallinity and uniform stoichiometric composition along the entire length of the nanowires. More importantly, the versatility of this doping scheme is illustrated by the fabrication of high-performance p-channel nanowire field-effect-transistors. High electrically active carbon concentrations of $\sim 7.5 \times 10^{17}$ cm^{-3} and field-effect hole mobility of ~ 140 cm^2 V^{-1} s^{-1} are achieved which are essential for compensating the electron-rich surface layers of InSb to enable heavily p-doped and high-performance device structures. All these further indicate the technological potency of this *in situ* doping technique as well as p-InSb nanowires for the fabrication of future CMOS electronics.

Introduction

In recent years, due to the unique physical properties, one-dimensional (1-D) semiconductor nanowires (NWs) have attracted extensive research attention as fundamental building blocks for next-generation electronic, optoelectronic and photovoltaic devices.[1–7] In particular, high mobility III–V NWs have been demonstrated with extraordinary device performances when configured as n-channel field-effect-transistors (FETs).[8–10] For instance, impressive electron mobilities up to 10 000 and 35 000 cm^2 V^{-1} s^{-1} have been achieved for InAs and InSb NWFETs contributing to one of the highest electron mobility values reported for the NW devices.[11,12] However, in addition to these n-type devices, p-channel FETs are also required for the practical design and implementation of NW based CMOS electronic circuits[2] while little work has been focused on the p-type InAs and InSb NWFETs till now. One challenge is related to the electron-rich surface layer existing in the intrinsic NW materials pinning the surface Fermi level in the conduction band which makes the p-type doping problematic and the realization of such high-performance p-channel devices difficult. Although techniques such as *in situ* as well as post-growth patterned doping have been studied for InAs NWs,[13–15] very few are performed on the equally important InSb NWs. In order to address this need, here, we present a simple synthesis technique and an effective approach of *in situ* p-doping of InSb NWs employing carbon dopants in the solid-source catalytic chemical vapor deposition. These grown NWs are stoichiometric, single-crystalline with a smooth surface and low defect densities. The versatility of this doping approach is also illustrated by configuring the doped NWs into p-MOSFETs while exhibiting high electrically active carbon concentration and field-effect hole mobility.

Experimental section

NW synthesis

InSb NWs studied in this work were grown by utilizing the solid-source chemical vapor deposition (CVD) in a tube furnace and the schematic illustration of the NW growth setup can be seen in ESI Fig. S1.† Briefly, a boron nitride crucible loaded with

[a]*Department of Physics and Materials Science, City University of Hong Kong, 83 Tat Chee Avenue, Kowloon Tong, Kowloon, Hong Kong, People's Republic of China. E-mail: johnnyho@cityu.edu.hk*

[b]*Department of Biology and Chemistry, City University of Hong Kong, 83 Tat Chee Avenue, Kowloon Tong, Kowloon, Hong Kong, People's Republic of China*

[c]*Shenzhen Research Institute, City University of Hong Kong, Shenzhen, People's Republic of China*

[d]*Department of Applied Chemistry, Kyung Hee University, Yongin, Gyeonggi, 446-701, Republic of Korea*

† Electronic supplementary information (ESI) available: Schematic illustration of the NW growth setup; SEM, EDS and transfer characterization of the intrinsically undoped n-InSb NWs; SEM of small diameter NWs; epitaxial growth of p-type InSb NWs from the $AuIn_2$ catalyst alloy; growth mechanism of Au-catalyzed carbon doped p-InSb NWs; lattice mismatch between undoped and C-doped NWs. See DOI: 10.1039/c3nr03080f

‡ These authors contributed equally to this work.

source materials was placed at the center of the quartz tube while growth substrates (Si wafer pieces with a 50 nm thick thermally grown oxide and a 2.5 nm thick Au catalyst film) were located in the downstream. Here, 1.00 g of InSb powders (99.999% purity) and 0.12 g of carbon powders (99.95% purity) were used for the p-InSb NW growth, detailed in the following sections, while 1.00 g of InSb powders (99.999% purity) and 0.30 g of In powders (purity 99.99%) were employed for growing the intrinsically undoped n-InSb NWs (see ESI Fig. S2†). Hydrogen (99.999% purity; 100 sccm) was used as the carrier gas to transport the thermally vaporized solid source downstream and the pressure was maintained at ~1 Torr for the entire duration. Prior to heating, the quartz tube was purged with H_2 for 0.5 h. After 2 h at a furnace temperature of 800 °C (the substrate temperature is measured ~400–475 °C by the k-type thermocouple), the grown substrates were then taken out of the furnace after reaching the ambient conditions.

NW characterization

Surface morphologies of the grown NWs were examined with a scanning electron microscope (SEM, FEI Company, Oregon, USA/Philips XL30, Philips Electronics, Amsterdam, Netherlands) and a transmission electron microscope (TEM, Philips CM-20). Crystal structures were determined by collecting X-ray diffraction (XRD) patterns on a Philips powder diffractometer using Cu Kα radiation ($\lambda = 1.5406$ Å), imaging with a high resolution TEM (HRTEM, JEOL 2100F, JEOL Co., Ltd., Tokyo, Japan) attached with the electron energy loss spectroscope (EELS, Gatan, Tridiem), energy dispersive X-ray spectroscopy (EDS) detectors and selected area electron diffraction (SAED) analysis. The chemical state of carbon dopants was also examined by X-ray photoelectron spectroscopy (XPS, ULVAC-PHI Inc., model 5802, Kanagawa, Japan). For the TEM, EELS and EDS studies, the NWs were first suspended in the anhydrous ethanol solution by ultrasonication and dropcast onto the Cu grid for the corresponding characterization.

FET fabrication and characterization

NWFETs were fabricated by drop-casting the NW suspension onto highly doped p-type Si substrates with a 50 nm thick thermally grown gate oxide. Photolithography was utilized to define the source and drain regions while a 50 nm thick Ni film was thermally deposited as the contact electrode followed by a lift-off process. The electrical performance of the fabricated back-gated FET was then characterized with a standard electrical probe station and an Agilent 4155C semiconductor analyzer (Agilent Technologies, California, USA).

Results and discussion

In general, it is well-known that tapering and surface coating are commonly observed in III–V NWs which are caused by the imbalance of the V/III precursor ratio supplied during the growth;[16] however, for this simple solid-source and *in situ* doping technique, the V/III ratio cannot be directly and independently controlled but can rather be tailored by adjusting the growth time and carrier gas flow together.[16,17] As depicted in the scanning electron microscopy (SEM) and transmission electron microscopy (TEM) images in Fig. 1a and b, very dense, long (>5 μm) and straight InSb NWs are successfully obtained with the optimized growth parameters on amorphous substrates (Si with a 50 nm thick thermally grown oxide), instead of the commonly used crystalline III–V substrates. Importantly, the NW diameters are uniform along the entire length of NWs and no tapering is observed, confirming the optimal control of processing parameters here. This well-controlled surface morphology is essential for the efficient gate coupling of subsequently fabricated p-type NW devices. From the statistics of 100 individual NWs from TEM images, the average diameter is determined to be 63 ± 18 nm in Fig. 1c and this narrow diameter distribution is remarkably good considering the simplicity of this growth scheme as compared to the sophisticated MBE and MOCVD system[10,12] and the variation of commercially available colloidal Au nanoclusters as catalysts for growing NWs. Smaller diameter NWs have been investigated with the use of thinner Au catalyst films as well; however, significant over-coating is observed which may be due to the Gibbs–Thomson effect (ESI Fig. S3†);[16,18] further studies on the thinner NWs *via* the manipulation of catalytic supersaturation[19] with different metal catalysts are currently in the process. At the same time, the crystal quality of as-grown NWs is also studied by X-ray diffraction (XRD) as presented in Fig. 1d. Based on the typical XRD spectrum, the observed peaks are identical to those of the zinc-blende crystal structure of InSb, having $a = b = c =$ 0.6782 nm (JCPDS Card, no. 06-0208), which is consistent with the selected area electron diffraction (SAED) result. Notably, most NWs studied by TEM are grown along the ⟨111⟩ directions while the phase purity is high such that no other phases (*i.e.* In_2O_3, In, C, Sb, *etc.*) are present in our NWs as indicated by

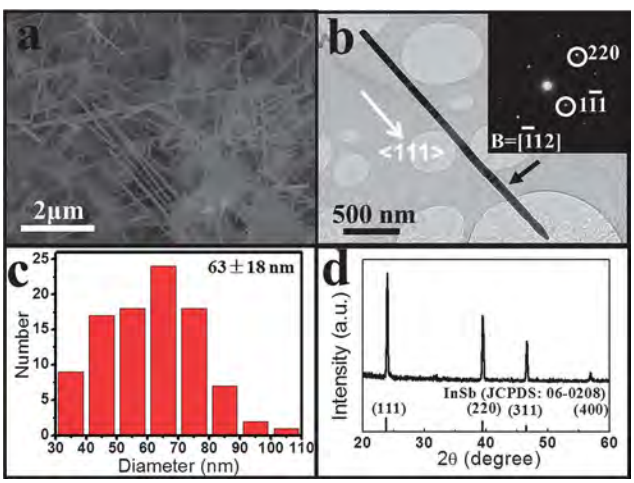

Fig. 1 (a) SEM; (b) TEM and SAED images of p-InSb NWs grown with the optimal process condition; (c) diameter statistics of 100 NWs observed in the corresponding TEM images. The grown NW has a smooth surface and a narrow diameter distribution; (d) XRD spectrum of the as-grown InSb NWs. (Optimal growth conditions: growth temperature at 800 °C, pressure at 1 Torr, gas flow rate at 100 sccm and duration of 2 h.)

XRD. All these further confirm the single-crystalline nature of p-doped InSb NWs obtained in this study.

In order to investigate the NW growth mechanism here, high-resolution TEM and energy-dispersive X-ray spectroscopy (EDS) analyses are performed in the as-grown NW catalyst/body region. As shown in Fig. 2, spherical and crystalline catalytic seeds can be clearly observed at the tips of all NWs while the body has a native oxide layer of ~5 nm. This is a distinct characteristic of vapor–liquid–solid (VLS) or vapor–solid–solid (VSS) growth mode. EDS line scan is then performed along the NW axial direction across from the tip to body. It is found that the catalyst mainly contains In and Au atoms (atomic ratio = 2 : 1) while the Au content drops drastically once passing the catalyst/NW interface. This observation suggests that no detectable Au diffusion occurs in the NW body which may damage the crystallinity and electrical properties. At the same time, the NW body consists of In and Sb elements in the atomic ratio of 1 : 1, suggesting that the stoichiometric InSb NWs are catalyzed by $AuIn_2$ alloy tips. Also, based on the plane spacing determination in the HRTEM imaging and corresponding reciprocal lattice spots extracted by fast Fourier transform (FFT), the NW has a catalyst/NW interface orientation relationship of cubic $AuIn_2${111}|cubic InSb{111} which again confirms the dominant growth axis of ⟨111⟩ in the NW body without any significant amount of crystal defects observed in HRTEM, such as stacking faults and inversion domains, *etc.* The NWs are preferentially grown along the ⟨111⟩ direction as this growth direction involves the lowest free energy crystal planes and thus it is more thermodynamically favorable.[20,21] At the same time, the lattice mismatch between $AuIn_2${111} and InSb {111} is insignificant as compared to other $AuIn_2$ orientations, such as {110} and {100} presented in ESI Fig. S4;† as a result, InSb NWs are preferable to grow epitaxially in ⟨111⟩ directions from $AuIn_2${111} oriented catalysts.[22] Notably, although carbon atoms are employed as p-type dopants in this work, they are expected not to involve in the NW nucleation here since carbon has an insignificant solid solubility in the Au catalysts.[23–26] Also, as reported by Salehzadeh *et al.*, carbon can incorporate through the triple boundary at the Au/NW interface;[27] as a result, Sb and carbon atoms are believed to react with In constituents (*i.e.* from the supersaturation of Au seeds) at the catalyst/NW interface for the formation and doping of NWs. More importantly, the presence of these carbon dopants is shown not to introduce any additional structural and stoichiometric defects affecting the NW crystal quality during the growth. The detailed growth mechanism is also summarized in ESI Fig. S5.†

Moreover, since the carbon dopants are small in their atomic size and cannot be characterized accurately by EDS, X-ray photoelectron spectroscopy (XPS) is utilized instead to confirm the existence of these carbon atoms as well as to assess their chemical states within the NWs. Fig. 3a gives the carbon 1s peak spectra for the InSb NWs grown on Si/SiO_2 compared to the signals from a bare substrate (without NWs). In the NW sample, the carbon 1s binding energy region exhibits predominately the non-oxidized carbon peaks at 283.1, 284.3 eV and an oxidized peak at 285.4 eV, corresponding to the C–In, C–C and C–O bonds, respectively, as reported in the literature (Fig. 3b).[28] The C–C and C–O bonds are believed to originate from the measuring atmosphere. In contrast, the bare substrate only shows similar peak locations for the C–C and C–O bonds except for the C–In bonds at 283.1 eV (Fig. 3c), indicating that carbon atoms are indeed introduced into the InSb crystal lattice,

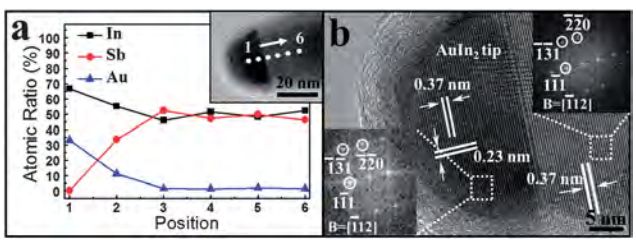

Fig. 2 (a) EDS line scan (measured from the position 1 to 6, as indicated by the white arrow in the inset) of a representative as-grown p-InSb NW tip region; (b) HRTEM image of the same NW and the inset shows the corresponding FFT images of the NW tip and body. (Tip: cubic $AuIn_2$ phase with JCPDS Card no. 03-0939; Body: cubic InSb phase with JCPDS Card no. 06-0208.)

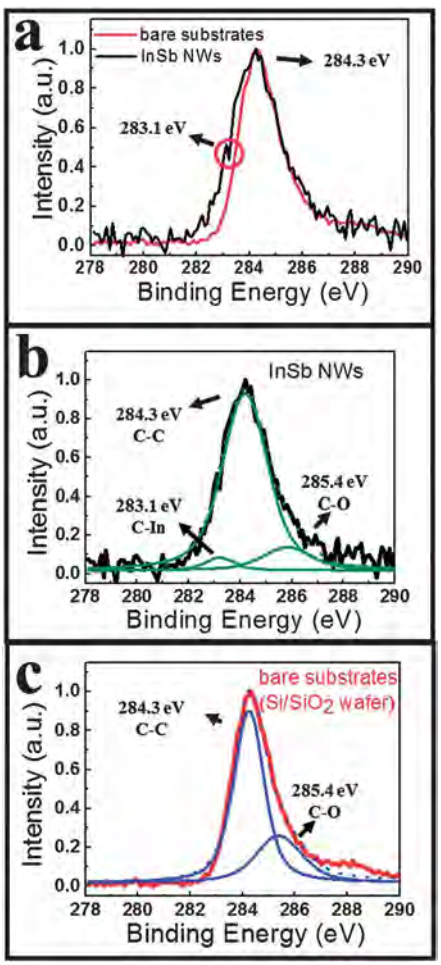

Fig. 3 (a) XPS spectra of the carbon 1s core region for the as-prepared carbon-doped InSb NWs grown on Si/SiO_2 and the bare substrate without NWs; (b) and (c) XPS peak fit for the NW samples and the bare substrate, respectively.

residing in the Sb sites and chemically bonded to the In atoms for this *in situ* p-doping scheme.

On the other hand, one of the challenges in synthesizing high-performance III–V nanowires is to control the NW stoichiometry uniformly and precisely to enable various device fabrications. Any dopant clustering or segregation would significantly degrade the electrical properties of NWs for high-performance device applications. In this regard, in addition to the surface sensitive technique of XPS, electron energy loss spectroscopy (EELS) is also employed to characterize the NW stoichiometric uniformity. As depicted in Fig. 4, the EELS elemental mapping of a representative NW demonstrates the homogeneous distribution of In, Sb and C atoms along the NW body axially. Although some fraction of C atoms may get deposited during the EELS measurement, combining with the high-resolution XRD studies (ESI Fig. S6†), the lattice mismatch between the undoped and C-doped NWs indicates the presence of substitutional carbon ($\sim 1.0 \times 10^{19}$ cm^{-3}) within the NWs. Notably, due to their small atomic size, carbon atoms are easily clustered or segregated during the doping process, affecting the resulting doping efficiency and crystal quality;[25,29–32] in any case, the uniform distribution of all constituents here illustrates the remarkably good control of the NW stoichiometry in the axial direction, consistent with the results obtained in the TEM analysis (Fig. 2). It should also be noted that more studies are in progress to further evaluate the carbon occupation in the NW radial direction in order to assess the surface *versus* bulk distribution of dopants and their effect on the corresponding NW electrical properties.

To shed light to investigate the electrically active content of carbon dopants as well as the electrical properties of doped NWs, common back-gated NWFETs are then fabricated and electrically characterized (Fig. 5a). The electrical performance of a representative FET consisting of an individual carbon-doped InSb NW as the channel material with the diameter of

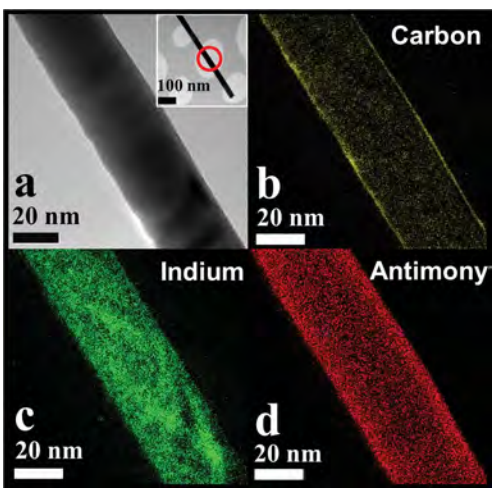

Fig. 4 (a) STEM image of a representative carbon-doped InSb NW. The inset shows the beam scanning area (red color circle) without any carbon film support on the TEM grid; (b–d) EELS elemental mapping of the NW in panel (a) for C, In and Sb atoms.

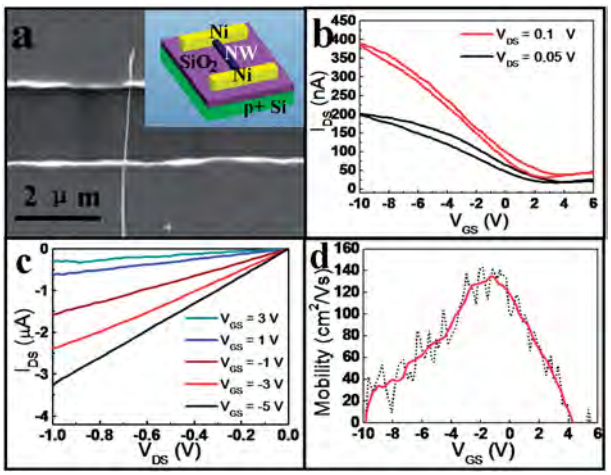

Fig. 5 (a) SEM image and (inset) schematic of a back-gated InSb NWFET with Ni metal contacts; (b–c) transfer and output characteristics of the representative NWFET with $d \sim 55$ nm and $L \sim 1.8$ μm; (d) mobility assessment under $V_{DS} = 0.05$ V of the device in panel (a).

$d \sim 55$ nm and a channel length of $L \sim 1.8$ μm is shown in Fig. 5b and c. As expected from the p-type doping of carbon, the NWFET exhibits p-channel characteristics and at $V_{DS} = 0.05$ V, it achieves 0.2 μA ON current under $V_{GS} = -10$ V and a 5 nA OFF current under $V_{GS} = 4$ V, in contrast to the intrinsically undoped n-type NWs and FETs as shown in ESI Fig. S2.† This ON/OFF current ratio (~ 50) is already one of the best reported values among most p-channel III–V NWFETs.[15] Also, the linear I_{DS}–V_{DS} behavior further confirms that the contacts to the p-InSb are near Ohmic here. This is primarily due to the thinning of the Schottky barriers at the contacts to the valence band of NWs arising from the heavy carbon doping. Moreover, the corresponding field-effect mobility is calculated as a function of V_{GS} (Fig. 5d). Specifically, the transconductance ($g_m = (dI_{DS})/(dV_{GS})|_{V_{DS}}$) at low bias $V_{DS} = 0.05$ V is assessed and the mobility is yielded by the standard square law model $\mu = g_m(L^2/C_{OX})(1/V_{DS})$, where C_{OX} is the gate capacitance obtained from the finite element analysis software COMSOL with respect to the different diameter of the nanowire. The calculated peak hole mobility is ~ 140 cm^2 V^{-1} s^{-1}, and based on a statistic of 20 devices, the average peak mobility is found to be 127 ± 21 cm^2 V^{-1} s^{-1}. This field-effect mobility is respectable and reasonable given that the hole Hall mobility of bulk InSb substrates for a doping concentration of $\sim 1 \times 10^{18}$ cm^{-3} acceptors is ~ 400 cm^2 V^{-1} s^{-1} at room temperature[33] while the measured Hall mobility is always larger than the extracted field-effect mobility.[34]

At the same time, the effective hole concentration, n_h, or the electrically active carbon content can also be extracted from the NW device characteristics. Using the conductance $G \sim 2.2 \times 10^{-6}$ S and $d \sim 55$ nm, the resistivity, $\rho \sim 0.06$ Ω cm, is estimated for the doped NW. From both ρ and μ determined at the same V_{DS} and V_{GS} values of 0.05 V and −2 V, respectively, the electrically active carbon concentration is found to be $\sim 7.5 \times 10^{17}$ cm^{-3}. This relatively high carbon concentration corresponds to the heavy doping, with the Fermi level E_F located close to the valence band edge E_v and this electrically active

carbon concentration is consistent with those reported for carbon dopants in bulk InSb films.[35,36] All these have illustrated the excellent p-channel device performance accomplished with this simple *in situ* carbon doping scheme. Notably, it would be fundamentally interesting to enhance the doping concentration and study their corresponding electrical properties while more investigation is currently in process.

Conclusions

In conclusion, a simple synthesis technique and an effective approach of *in situ* carbon-doping of InSb NWs on amorphous substrates is presented and confirmed by the comparison with the intrinsically undoped n-type NWs. The grown p-InSb nanowires have remarkable single crystallinity as well as uniformly distributed stoichiometric composition of their constituents and dopants axially. By fabricating back-gated p-channel field-effect transistors, the respectable ON/OFF current ratio (~50), high hole mobility (~140 $cm^2 V^{-1} s^{-1}$) and electrically active dopant concentration (~7.5×10^{17} cm^{-3}) are obtained, demonstrating the success of incorporating and activating carbon dopants in the NW channel with this doping scheme. All these indicate the technological potency of our p-InSb NWs for the future fabrication of high-speed and low power complementary metal–oxide–semiconductor field-effect-transistors based on III–V nanowires.

Acknowledgements

This research was supported by the General Research Fund of the Research Grants Council of Hong Kong SAR, China, under project numbers CityU 101111, the National Natural Science Foundation of China (grant number 51202205), a grant (JCYJ20120618140624228) from the Shenzhen Research Institute, City University of Hong Kong and Basic Science Research Program through the National Research Foundation of Korea (NRF) funded by the Ministry of Science, ICT & Future Planning (NRF-2012R1A1A1015659).

Notes and references

1 M. S. Gudiksen, L. J. Lauhon, J. Wang, D. C. Smith and C. M. Lieber, *Nature*, 2002, **415**, 617.
2 J. A. del Alamo, *Nature*, 2011, **479**, 317.
3 J. W. Jiang, J. S. Wang and B. W. Li, *Nanoscale*, 2010, **2**, 2864.
4 J. J. Hou, N. Han, F. Wang, F. Xiu, S. Yip, A. T. Hui, T. Hung and J. C. Ho, *ACS Nano*, 2012, **6**, 3624.
5 E. Russo-Averchi, M. Heiss, L. Michelet, P. Krogstrup, J. Nygard, C. Magen, J. R. Morante, E. Uccelli, J. Arbiol and A. F. i Morral, *Nanoscale*, 2012, **4**, 1486.
6 P. M. Wu, N. Anttu, H. Xu, L. Samuelson and M. E. Pistol, *Nano Lett.*, 2012, **12**, 1990.
7 S. W. Ma, Q. L. Liao, H. S. Liu, Y. Song, P. Li, Y. H. Huang and Y. Zhang, *Nanoscale*, 2012, **4**, 6415.
8 A. C. Ford, J. C. Ho, Z. Fan, O. Ergen, V. Altoe, H. Razav and A. Javey, *Nano Res.*, 2008, **1**, 32.
9 A. T. Vogel, J. de Boor, J. V. Wittemann, S. L. Mensah, P. Werner and V. Schmidt, *Cryst. Growth Des.*, 2011, **11**, 1896.
10 C. Thelander, P. Caroff, S. Plissard and K. A. Dick, *Appl. Phys. Lett.*, 2012, **100**, 232105.
11 A. C. Ford, J. C. Ho, Y. L. Chueh, Y. C. Tseng, Z. Fan, J. Guo, J. Bokor and A. Javey, *Nano Lett.*, 2009, **9**, 360.
12 S. R. Plissard, D. R. Slapak, M. A. Verheijen, M. Hocevar, G. W. G. Immink, I. van Weperen, S. Nadj-Perge, S. M. Frolov, L. P. Kouwenhoven and E. P. A. M. Bakkers, *Nano Lett.*, 2012, **12**, 1794.
13 H. Y. Li, O. Wunnicke, M. T. Borgström, W. G. G. Immink, M. H. M. van Weert, M. A. Verheijen and E. P. A. M. Bakkers, *Nano Lett.*, 2007, **7**, 1144.
14 J. C. Ho, A. C. Ford, P. W. Leu, Y. L. Chueh and A. Javey, *Appl. Phys. Lett.*, 2009, **95**, 072108.
15 A. C. Ford, S. Chuang, J. C. Ho, Y. L. Chueh and A. Javey, *Nano Lett.*, 2010, **10**, 509.
16 N. Han, F. Y. Wang, A. T. Hui, J. J. Hou, G. C. Shan, X. Fei, T. F. Hung and J. C. Ho, *Nanotechnology*, 2011, **22**, 285607.
17 A. T. Hui, F. Y. Wang, N. Han, S. P. Yip, F. Xiu, J. J. Hou, Y. T. Yen, T. F. Hung, Y. L. Chueh and J. C. Ho, *J. Mater. Chem.*, 2012, **22**, 10704.
18 M. Ek, B. M. Borg, J. Johansson and K. A. Dick, *ACS Nano*, 2013, **7**, 3668.
19 N. Han, F. Wang, J. J. Hou, S. P. Yip, H. Lin, M. Fang, F. Xiu, X. Shi, T. F. Hung and J. C. Ho, *Cryst. Growth Des.*, 2012, **12**, 6243.
20 S. G. Ihn, J. I. Song, T. W. Kim, D. S. Leem, T. Lee, S. G. Lee, E. K. Koh and K. Song, *Nano Lett.*, 2007, **7**, 39.
21 S. A. Fortuna, J. Wen, I. S. Chun and X. Li, *Nano Lett.*, 2008, **8**, 4421.
22 N. Han, A. T. Hui, F. Y. Wang, J. J. Hou, F. Xiu, T. F. Hung and J. C. Ho, *Appl. Phys. Lett.*, 2011, **99**, 083114.
23 T. B. Massalski, H. Okamoto, P. R. Subramanian and L. Kacprzak. *Binary alloy phase diagrams*, William W. Scott, Jr, USA, 1990, p. 346.
24 A. Maiti and A. Ricca, *Chem. Phys. Lett.*, 2004, **395**, 7.
25 K. Asaka, M. Karita and Y. Saito, *Appl. Surf. Sci.*, 2011, **257**, 2850.
26 Y. Zhang, N. W. Franklin, R. J. Chen and H. Dai, *Chem. Phys. Lett.*, 2000, **331**, 35.
27 O. Salehzadeh, X. Zhang, B. D. Gates, K. L. Kavanagh and S. P. Watkins, *J. Appl. Phys.*, 2012, **112**, 094323.
28 C. D. Wanger, W. M. Riggs, L. E. Davis and J. F. Moulder, *Handbook of X-ray Photoelectron Spectroscopy*, G. E. Muilenberg Perkin-Elmer Corp., Eden Prairie, Minnesota, USA, 1979, p. 190.
29 E. F. Schubert, *Doping in III-V Semiconductors*, Cambridge University Press, Cambridge, UK, 1993, p. 190.
30 S. Nozaki, K. Takahashi, M. Shirahama, K. Nagao, J. Shirakashi, E. Tokumitsu and M. Konagai, *Appl. Phys. Lett.*, 1993, **62**, 1913.
31 H. C. Kuo, D. Ahmari, B. G. Moser, J. Mu, M. Hattendorf, D. Scott, R. Meyer, M. Feng and G. E. Stillman, *J. Vac. Sci. Technol., B*, 1999, **17**, 1185.
32 H. Sohn, E. R. Weber, S. Nozaki, M. Konagai and K. Takahashi, *Mat. Res. Soc. Symp. Proc.*, 1992, **262**, 129.

33 J. D. Wiley, R. K. Willardson and A. C. Beer, *Semiconductors and Semimetals*, Academic Press, New York, 1975, p. 91.
34 L. Botha, P. Shamba and J. R. Botha, *Phys. Status Solidi C*, 2008, **5**, 620.
35 W. V. Schoenfeld, M. J. Antonell and C. R. Abernathy, *Appl. Phys. Lett.*, 1998, **72**, 1235.
36 H. T. Pham, S. F. Yoon, K. P. Chen and D. Boning, *J. Phys. D: Appl. Phys.*, 2008, **41**, 025304.